Natural Hazards (2023) 117:2347–2373
https://doi.org/10.1007/s11069-023-05945-8

ORIGINAL PAPER

Debris and mud flows runout assessment: a comparison among empirical geometric equations in the Giampilieri and Briga basins (east Sicily, Italy) affected by the event of October 1, 2009

Luca Maria Falconi[1] · **Lorenzo Moretti**[2] · **Claudio Puglisi**[1] · **Gaia Righini**[2]

Received: 15 November 2022 / Accepted: 24 March 2023 / Published online: 15 April 2023

Abstract
Empirical/geometric methods rely on simple geometrical connections between some landslide parameters and the runout distance reached by the displaced material. Despite the extreme simplification of the dynamic of this landslide typology, those methods can provide useful information about the propagation of this shallow and fast landslide typology, joining the reliability of the results with easiness of use. The objective of this work is to compare the efficacy of different geometric relationships for the identification of the runout distances in a debris- and mud-flows-prone test area located in Sicily, southern Italy, where several events were analyzed, and a consistent set of data was collected and processed. Notwithstanding some uncertainties in the methodological approach and not negligible scattering between expected and observed runout distances, the use of such geometric approaches, together with the evaluation of kinematic parameters such as velocity and kinetic energy, can significantly boost the implementation of site-specific analyses for a more detailed definition of landslides susceptibility at a local scale.

Keywords Runout · Debris flows · Geometric approach · Messina · Italy

Abbreviations

GIS	Geographic information system
IA	Initiation area
TP	Toe point

✉ Luca Maria Falconi
luca.falconi@enea.it

Lorenzo Moretti
lorenzo.moretti@enea.it

Claudio Puglisi
claudio.puglisi@enea.it

Gaia Righini
gaia.righini@enea.it

[1] ENEA - Casaccia R.C, Via Anguillarese 301, Rome, Italy

[2] ENEA - Bologna R.C, Via Martiri Di Monte Sole 4, Bologna, Italy

LEWS	Landslides early warning system
LIP	Landslide identification point
LP	Landslide path
TA	Track area
SBP	Slope break point

1 Introduction

Debris and mud flows, shallow and fast-moving landslides involving plastic and saturated material (Hungr et al. 2014), start on steep slopes while the displaced material could be carried also very far from the initiation areas. Usually, the landslides hazard and risk maps implemented by regional and local authorities mainly include the inventory maps of past landslide and/or landslide susceptibility maps showing the potential initiation areas, i.e., areas of the initial detachment of the landslides. Regional hazard maps provided by public authorities rarely are the result of debris flows runout analysis. In these fundamental land planning instruments, the determination of the area that may be reached by the displaced material and the lower point of the debris deposition area, where most elements at risk are typically located, is often missing. Joining the identification of landslide source area with its runout, the distance covered by the displaced material, and the propagation area allows a more exhaustive comprehension of the phenomena and more efficient hazard and risk assessment (Corominas et al. 2003; Melo and Zezere 2017).

The propagation of the material detached by debris and mud flow is a combination of several causes and elements, extremely difficult to reproduce and analyze in appropriate and exhaustive models. Two main types of procedures are widely used for the runout investigation: empirical–statistical expressions, mainly based on the correlation of geometric parameters, and analytical/numerical models that simulate several parameters of the physical processes (Rickenmann et al. 2005; Hürlimann et al. 2008; McDougall 2017). The distinction between the two approaches is not always sharp because some empirical relations are often used in the simulation procedures due to the difficulties in gathering simple and universal rules for landslides modeling (Scheidl and Rickenmann 2010; Pastor et al. 2012; Huang and Cheng 2017).

The extension of the study area and the objective of the investigation usually drive the choice between the two approaches, involving different details, scales and engaged efforts. While the location and definition of stabilization structural works need a slope scale description and analysis, the implementation of tools for the regional planning and early warning system design requires the description of huge dataset, spread on a wide area. Moreover, the design of an early warning system needs necessarily to join the appraisal of the initiation susceptibility with the estimate of the material propagation. The numerical modeling approach is specifically suitable to characterize a single event and to design the actions at slope scale, even if recent studies illustrate some more extended application (Di Napoli et al. 2021; Guthrie and Befus 2021). The neural networks were also used to estimate the runout with promising results that could be improved by adding further and wider dataset (Chae et al. 2006).

Empirical/geometric methods rely on simple correlations between some landslide parameters and runout (Hungr 1995; Jakob and Hungr 2005; Fig. 1). Despite the extreme simplification of the dynamic of the phenomena under investigation, those methods can

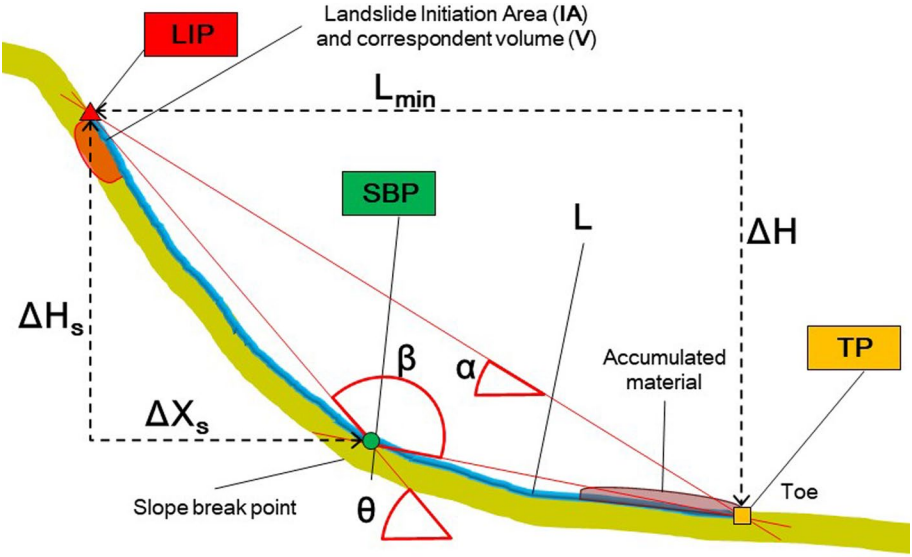

Fig. 1 Main elements related to the runout assessment of a debris flow. Landslide initiation point: maximum height of the main scarp. Toe point: lower point of the accumulated material; slope break point: point where significantly change the slope gradient; L: 3D runout distance; L_{min}: 2D runout distance; ΔH: height difference between the top of the main scarp and the toe; ΔH_s: height difference between LIP and SBP; ΔX_s: planar distance between LIP and SBP; α: reach (or extension, propagation) angle; θ: slope angle; β: transition angle

provide a prediction of the extent of the landslide propagation with good reliability (Berti and Simoni 2007). Moreover, they can successfully support decision-makers and are consistent with more recent guidelines for landslides risk assessment (Porter and Morgenstern 2013; Corominas et al. 2014).

The first and most used empirical expression in the geometrical approach is based on the "reach angle—Fahrböschung," introduced by Heim (1932), which links the vertical drop with the roughness of the terrain below the initiation zone (i.e., obstacles, rock walls, trees), the friction coefficient of the detached material and the landslide volume (Zou et al. 2017). A general regression Eq. (1) describes the relationship where A and B are constants and V is the landslide volume:

$$log(tan\alpha) = A + BlogV \tag{1}$$

Using this equation, in the past decades some authors have analyzed several datasets of debris flow events that occurred in different areas of the world, obtaining different values of the constants (Corominas 1996; Crosta et al. 2003; Lorente et al. 2003; McDougall, 2014).

Highlighting the potential energy component, the general relationship was expressed in a slightly different form by Rickenmann (1999) and García-Ruiz et al. (2002):

$$L = 30(MH)^{0.25} \tag{2}$$

where the runout (L) is in relation to the mass (M) of the displaced material and the difference in height (H) between the highest point of the debris flow (LIP) and the lower point of the landslide deposit toe (TP). Even if the runout is clearly correlated with the landslide

height, this relation cannot be easily applied in forecast analysis because the stopping point of the material is obviously unknown a priori, being instead the parameter to identify. Anyhow, the strong correlation between the runout and the volume suggested a direct and suitable connection that was applied in Legros 2002.

As several parameters influence the landslide movement, the runout forecasting models should consider concurrently as much influence factors as possible. In Guo et al. (2014), the results of the multiple factor predictive methods applied on 54 landslides (mainly rock soil slides and debris rock avalanches), triggered by the 2008 Wenchuan earthquake, show that the type of rock, the volume detached in the initiation area and the transition angle on the slope, have a prevalent effect on the propagation distance. Guo analysis highlights how crucial is in this landslide process the transition angle that depends on the slope angle above and below the point along the landslide path which significantly changes the slope gradient, below which the velocity of the phenomenon decreases and where the debris flow gradually loses the erosion power and the deposition starts. Starting from Eq. (2), another expression (Puglisi et al. 2015) focused on the role played by the initial portion of the slope, using its height instead of the total vertical drop of the landslide.

In several and widespread situations, especially in developing countries, the lack of good quality datasets, the scarcity of funds and the absence of expert staff are serious drawbacks for landslide susceptibility and risk assessment, in particular using advanced numerical models. Therefore, the implementation of simple and low-cost methodologies, easily applicable and reliable is an urgent and required need (Guinau et al. 2007), also in the runout estimation of debris and mud flow. One of the most powerful innovations of the GIS tools for data processing (such as the "Model Builder" in ArcGIS or "Graphic Modeller" in QGIS) can facilitate large area analyses that require the execution of numerous algorithms in sequence to achieve the identification of the landslide path and the runout distance from a specific starting point. In this framework, starting from a potential source areas map, the geometric approach is especially useful to implement tools devoted to regional planning and (pre)early warning system design.

The objective of this work is to compare the efficacy of different geometric expressions for the identification of the runout of debris and mud flows in a test area located in Sicily, southern Italy, where several events were analyzed, and a consistent dataset was collected and processed by means of the GIS tools available in QGIS open software. The debris and mud flows used as a base dataset in the present study occurred along an area on the Ionian side of the Peloritani Mountain Belt, SW of Messina Italy (Fig. 2), hit by a high concentrated rainstorm on the October 1, 2009. This intense rainfall event triggered abundant slope failures, mainly debris and mud flows, in the southern Messina municipalities, Itala and Scaletta Zanclea areas causing severe damages in small villages and along the transportation network; unfortunately, also many fatalities and injured people were reported (Regione Siciliana 2009; Fig. 3).

2 Regional setting

The Peloritani Mountain Belt is the southern extremity of the Calabride-Peloritan Arc in the Nord-East Sicily and a SE verging pile of nappes composes it. Pre-Alpine metamorphic units that were involved in Hercynian and Alpine orogenic processes and overlap sedimentary Maghrebid units (Carbone et al. 2007) characterize each nappe. Outcropping formations in the Peloritanian sector are mostly composed of micashists of various metamorphic

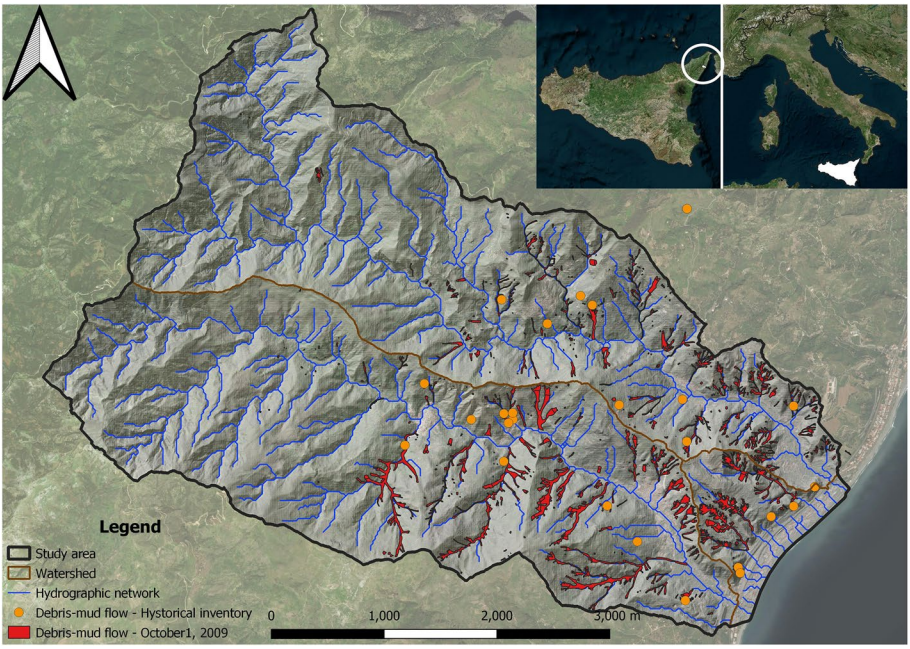

Fig. 2 Debris-mud flows inventoried in the study area distinguished in hystorical (orange dots) and occurred in October 1, 2009 (red areas) events

Fig. 3 Debris and mud flows in the Messina municipality area

grades and secondly by deposition of sedimentary covers. The fast crustal uplifts, starting from the upper Pliocene and lower Pleistocene, strongly influenced the overall geomorphology, which resulted in a high energy relief, "V"-shaped valleys with steep slopes eroded by torrent-like straight watercourses, narrow and deeply embanked into high rock walls in the mountain sectors, becoming wide and over-flooded in the terminal parts with extensive alluvial fans or dejection cones, ruins of old cliffs, fluvial and marine terraces (Regione Siciliana 2004). The low geomorphologic evolution, typical of a recent uplift, fosters intensive erosion processes and the alteration and degradation of crystalline lithotypes, as well as the high erodibility of sedimentary deposits, cause a widespread instability along the slopes. During high-intensity and prolonged hydrometeorological events,

gravitational movements classified as rapid mud and debris flows occur. These rapid flows start on neoformation rupture surfaces as small roto-translational slides in the soil over the bedrock and then become mud and debris flows which move toward the valley with a velocity of several meters per second (about 10 or 15 m/s).

Mica schists, phyllites and sericitic-chloritic schists compose the bedrock parent material of the detached soil. The soil thickness is variable according to the terraces preservation status and its contact with the bedrock varies in depth from 50 to 80 cm. The soils are usually sandy with low clay content (almost 10%) and clearly show thixotropic characteristics (Napoli et al. 2015). Brown soils—Rankers—lithosols outcrop in the most elevated side of the area, close to the Peloritani watershed, while brown soils—leached brown soils—lithosols outcrop in the highest portions of the coastline (Ballatore & Fierotti 1967). Leptic Cambisols ed Eutric Cambisols (Sodic) are present in the most elevated and medium parts of the slopes characterized by abandoned/not preserved terraces and currently covered with mixed bushed vegetation.

Orographic and morphologic characteristics as a whole directly influence the climatic features of the territory near Messina, typically Mediterranean with hot and dry summers, and precipitation falling mostly in the period from October to January. The mountain range close to the coastline, which represents a barrier for the air masses coming from Tyrrhenian and Ionian seas, strongly conditions the pluviometric trend (Nigro, 2011). Rainfall events are usually short and intense during the rainy season (October–April) and quite rare in the dry season (May–September). The October 1, 2009 precipitation is not an unusual event in the area of interest: some similar events have been recorded before (29–30 October 1985, 3–4 October 1996, 25 October 2007) and after (10th of March 2010, 22nd of November 2011, 1st of November 2012) even if they caused minor consequences. From the 15th and the 16th of September 2006, an event with 199 mm in 3 h rainfall intensity was registered; despite the higher intensity in comparison with the October 1, 2009 event (162 mm in 7 h), it didn't trigger significant landslides. More recently, from 24 and 26 October 2021, some exceptional events with Civil Protection warning communications were recorded.

Landslide hazard in Messina municipality, which experienced also widespread fires in the past, lead often to a generalized high risk due to the specific urbanization and the poor availability of hydro-geomorphologic risk reduction plans. A continuous urban landscape along the coastline, where the population migrated in the past decades leaving the outback original settlements, characterizes the study area. Moreover, several critical linear infrastructures are located along the coastline, such as main highways, railways, pipelines, and telecommunication features. Inland and most elevated areas, used in the past for grazing and agriculture, are now covered by woods, shrubs, and meadows, while in the hills and valleys prevail areas devoted to different agriculture activities.

In the past ten years, after the October 1, 2009 event, many studies analyzed the geomorphologic hazard of the area of interest, paying special attention to the rapid shallow landslides. Beyond landslides inventories (Ardizzone et al. 2012; Ciampalini et al. 2015; Malerba et al. 2015), several studies considered the hydraulic aspects of debris flows and the relationships with rapid floods (Casalbore et al. 2011; Aronica et al. 2012; Fiorillo et al. 2018), or specifically landslides hazard (Nigro et al. 2011; Puglisi et al. 2013) and related geomorphologic (De Guidi and Scudero 2013) and anthropic (Del Ventisette et al. 2012) control factors. A significant effort was devoted to debris flow susceptibility analysis based on physical (Schilirò et al. 2015a), deterministic (Schilirò et al. 2015b), and statistics (Lombardo et al. 2018) models. Moreover, some

work was dedicated to setting up the first steps of local landslides early warning and environmental protection systems (Basile & Panebianco 2011).

3 Material and methods

In addition to Eq. (2), the analysis is focused on other empirical geometric equations that relate one or more dimensional characteristics of a debris–mud flow to the runout. The Legros (2002) equation, characterized by an extreme simplicity and ease of application, was also taken into consideration:

$$L = 235V^{0.39} \tag{3}$$

which relates the runout distance L to the displaced volume V. On the contrary, Guo et al. (2014) equation is substantially more complex:

$$\log L_{max} = 0.136RT + 0.159\log V + 0.529\sin\beta + 1.497 \tag{4}$$

where, in addition to the volume and the transition angle (β) in the slope break point (SBP), also the type of rock involved in the movement—RT factor—is considered.

Also, the equation in Puglisi et al. (2015) considers the change in the slope gradient along the landslide path:

$$L = a(V * \Delta H_s)^b \tag{5}$$

The general relationship has been applied for two distinguished dataset of confined and unconfined debris flows (respectively mud–debris flow and debris avalanche sensu Hungr et al. 2014), providing two distinct power functions, respectively:

$$L = 5.049\left(V * \Delta H_s\right)^{0.329} \quad \text{confined} \tag{6}$$

$$L = 3.099\left(V * \Delta H_s\right)^{0.346} \quad \text{unconfined} \tag{7}$$

The confined elements represent those phenomena that along the path merged into a preexisting drainage line, while the unconfined propagated on an open slope. In the first case, the landslides maintained approximately the same width as the initiation areas, while in the second case they increased significantly their width moving downstream (Hungr et al. 2013).

Agreeing with the key role played by the SBP in the propagation dynamics of a displaced mass but focusing more on the gradient than on the height of the initial portion of the slope, a new further equation is developed and proposed in the present work:

$$L = a(V * i)^b = a\left(\frac{V * \Delta H_s}{\Delta X_s}\right)^b \tag{8}$$

where, in addition to the volume, the runout is correlated with the gradient of the slope between the LIP and the SBP, equal to the ratio between the height (ΔH_s) and the length (ΔX_s) of the initial part of the slope.

The analysis began with the results of geomorphological field surveys and aerial photo observation (October 1, 2009 post-event flights acquisition provided by the Civil Protection Office of the Messina Municipality), collected in an inventory of about

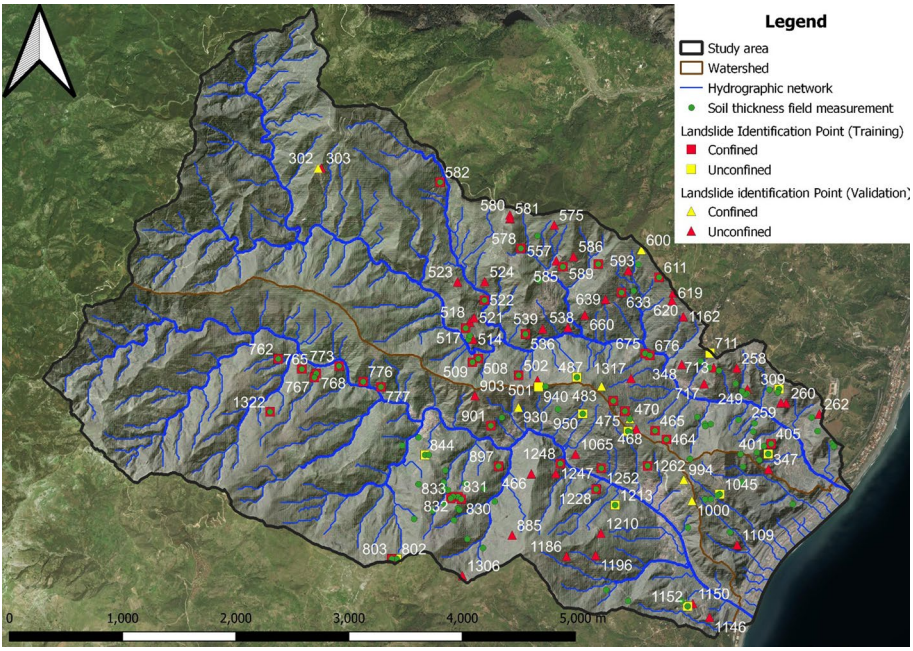

Fig. 4 Study area with the 100 observed Landslide Identification Points (50 for training and 50 for validation analysis), distinguished in confined (red dot) and unconfined (yellow dot). The 114 points (green) where the soil thickness were measured are also shown

two-thousand debris and mud flows occurred in the Messina area between 2007 and 2011. One hundred elements, distinguished in confined (19) and unconfined (81), were extracted from the inventory, mainly randomly, in order to constitute a representative subset of all known rapid shallow landslides of the area (Fig. 4). Fifty of these (12 confined and 38 unconfined) were used ad training dataset to identify site-specific runout equations while the remaining fifty (7 confined and 43 unconfined) were used for the validation of the equations. While the calibration dataset was mainly randomly selected from the surveyed data provided with all the necessary geometric and soil thickness parameters, the validation dataset was selected with greater attention avoiding the phenomena with particularly lobed shapes, a long path clearly channeled into the drainage network and evident interactions with anthropic structures.

In addition to the LIP and the TP, the Initiation Area (IA, polygonal element related to the source area) and the Landslide Path (LP, linear element representative of the path between LIP and TP and consequently of the runout) the vector layers have been drawn for each of the 100 observed events (Figs. 5 and 6). On the basis of geomorphological interpretation of the aerial photographs, the polygon of each Initiation Area has been drawn having as main references the crown of the main scarp. Because of the difficulty in the unique identification of the toe of the rupture surface, many of the inventoried areas resulted useless for the aim of the study. In addition to the elements used in the study, the Track Area (area affected by the flow along the path) and the Deposition Area (zone of accumulation at the foot of the landslide) were also delineated.

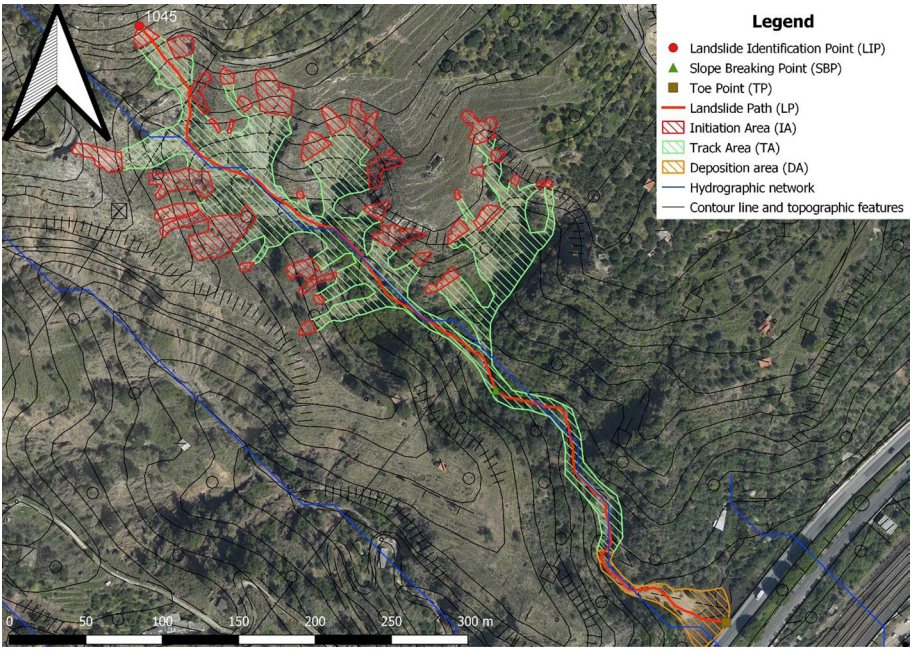

Fig. 5 Characteristic geometric elements in a wide but confined debris–mud flows system

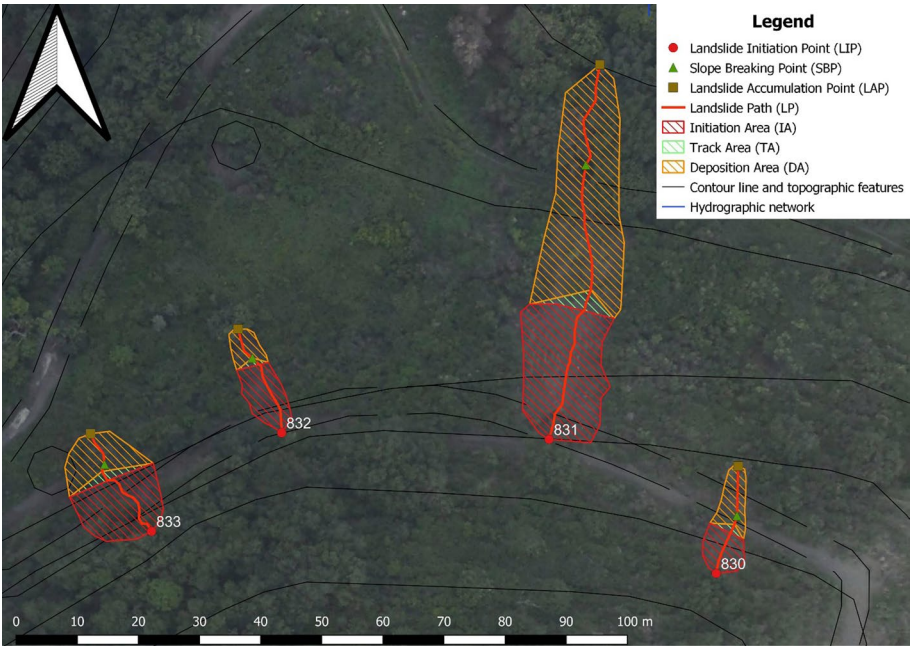

Fig. 6 Characteristic geometric elements in four adjacent unconfined debris–mud flows

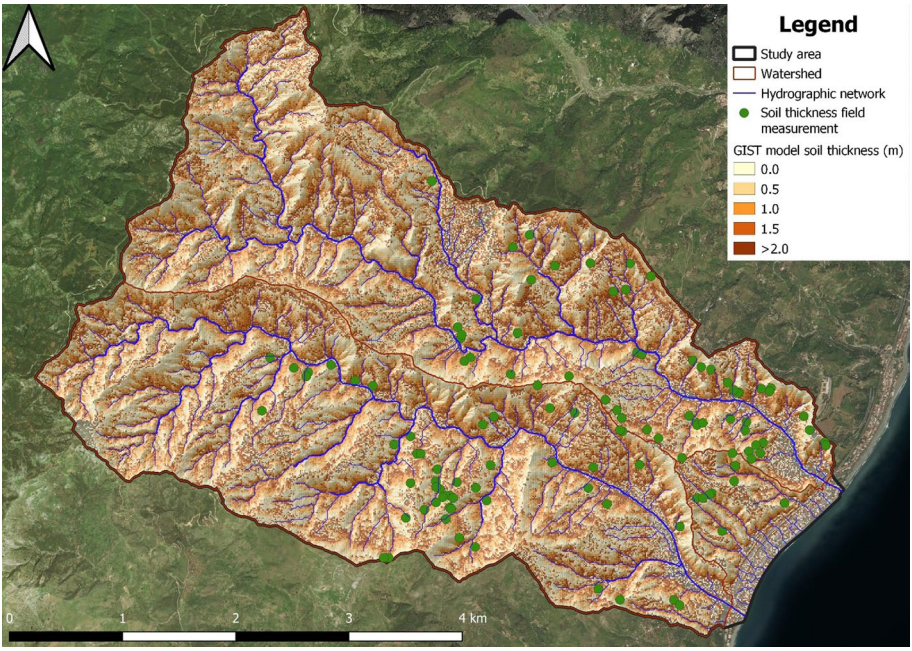

Fig. 7 Soil thickness map produced with the GIST model equation with the 2 m cell size DEM

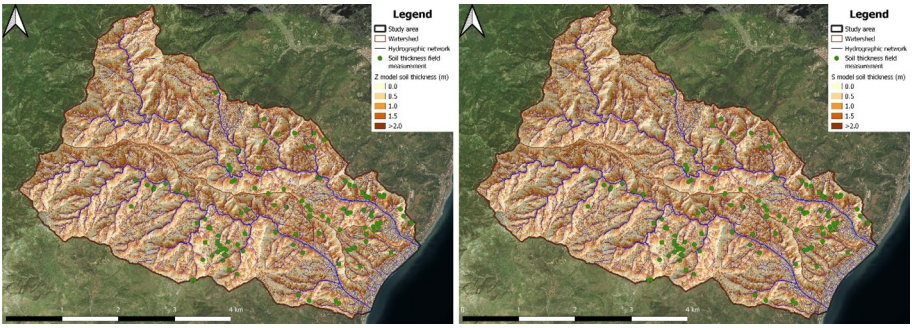

Fig. 8 Soil thickness map produced with the Z (left) and S (left) model equation with the 2 m cell size DEM

Using the 2 m cell size DEM (derived by the aerial photograph interpretation), the absolute height (m a.s.l.) of each element of the two punctual layers (LIP and TP) was identified, while for the linear layer (LP) the length (m) was calculated, both in plan (2D) as on the DEM (3D). The volume (m^3) of each landslide has been calculated through the areal layer (IA; m^2), and the soil thickness (m) map was produced using the GIST model equation (Catani et al. 2010; Fig. 7):

$$h_i = -Kc \bullet C \bullet \eta \bullet \psi^{-1} \tag{9}$$

where h_i represents the soil thickness, K_c is a calibration parameter that adjusts the normalized values of the other indices to real thickness values, C is an index linked to the slope curvature, η is an index linked to the position along the slope profile and ψ is linked to the critical slope threshold. In addition to the GIST modeling approach, the calculation of the soil thickness was also carried out with the Z and S models equation (Saulnier et al. 1997; Fig. 8):

$$h_i = h_{max} - \frac{\left(z_i - z_{min}\right)}{\left(z_{max} - z_{min}\right)}\left(h_{max} - h_{min}\right) \quad \text{(10 [Z model])}$$

$$h_i = h_{max}\left[1 - \frac{tan\theta_i - tan\theta_{min}}{tan\theta_{max} - tan\theta_{min}}\left(1 - \frac{h_{min}}{h_{max}}\right)\right] \quad \text{(11 [S model])}$$

In these equations h_i, z_i and θ_i indicate, respectively, the soil thickness, the elevation and the slope at the ith cell, while $h_{\max}$, $h_{\min}$, $z_{\max}$, $z_{\min}$, $\theta_{\max}$ and $\theta_{\min}$ are the maximum and minimum values, respectively, of the soil thickness, elevation and slope measured in the study area. Based on an estimate supported by field observations, minimum and maximum values of the soil thickness have been, respectively, attributed to 0 and 2 m.

While the two "topographic models" are very simple to apply, the soil thickness estimation through the GIST model required the development of a complex process aimed at the definition of the four indices using the 2 m cell size DEM.

The C index was produced as a normalization of the longitudinal curvature derived from the DEM. The morphological characteristics of the slopes of the study area were equalized to cases 1 (convex profiles) and 2 (convex to concave profiles) described in Catani et al. (2010), in which the C index is inversely proportional to the curvature.

Firstly, the definition of the η index required the calculation of the parameter P (length of the upstream flow/length of the total flow), through the use of the GRASS "r.flow" tool, applying the 3D option. The metamorphic and sedimentary formations, prevalent in the outcrops in the study area, were treated in analogy to the toposequence of the flyscioid and crystalline units of the Terzona basin (Catani et al. 2010). In this type of toposequence, the index η is set equal to the parameter P, assuming that η increases linearly from the minimum value ($\eta = 0$) in correspondence with the talweg ($p = 0$) to the maximum ($\eta = 1$) in correspondence with the watersheds ($p = 1$).

The ψ index was defined starting from the elaboration of the slope values and the lithotechnical characteristics in correspondence with the inventoried LIP of the event of October 1, 2009. Slightly higher values than the internal friction angle of the three lithotechnical classes (Granular B, Stratified A and Crystalline) affected by the debris flows have been attributed to the index ψ, as critical slope angles.

Once all the levels (in raster format) relating to the C, η and ψ indices were developed, the calibration factor Kc was identified, carried out by identifying the minimum value of the sum of the square of the difference between the in-field measured value and the calculated.

The results of the three models offer a different distribution in the soil depth classes (Fig. 9). The Z and S models indicate an unrealistic prevalence of the 1–2 m soil thickness class meanwhile the GIST model offers a more realistic distribution, exceeding the maximum estimated value of 2 m for the 17% of the cells in the area.

The results were also compared with 114 in-field measured data (Fig. 10). While the Z and S models overestimate the soil thickness, the results of the GIST model show errors

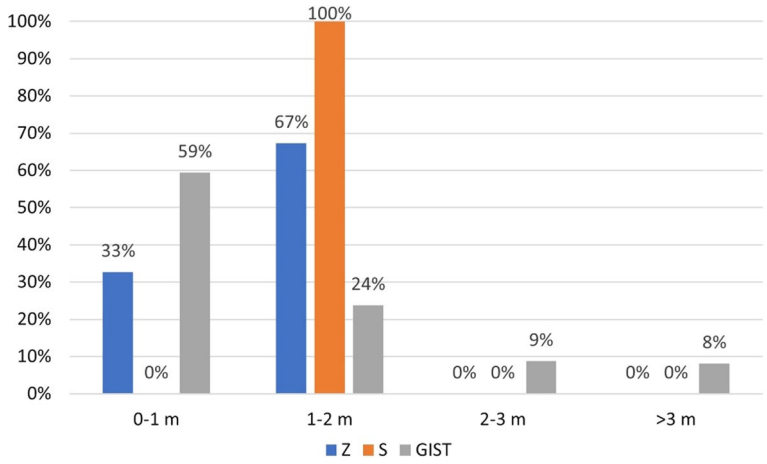

Fig. 9 Soil thickness distribution of the Z, S and GIST models

that are not small but more balanced (34% > 0 and 66% < 0), the average Δ value (average value of the difference between estimated and measured thickness) equal to − 20 cm and the standard deviation equal to 0,84. Though it widely shows considerable discrepancies, even greater than one meter, the GIST soil thickness map was deemed adequate for the aim of the study and thus used in the subsequent elaborations. The low accuracy was considered acceptable, especially because the error introduced would still be applied homogeneously on each of the runout equations.

The volume of each of the 50 polygons of the training dataset was calculated in four ways, all using the soil thickness map provided by the GIST model:

I. VCT—using a map algebra tool (volume calculation tool of QGIS) to estimate, cell by cell, the volume of soil, that was then summed up inside the initiation areas (IA),
II. VCT* k_h—using the same QGIS tool but with a correction factor k_h (see Eq. (12)),
III. d_{ave}*A—as product between initiation area (IA) and the average value of the GIST soil thickness map (d_{ave}) in the source area
IV. d_{max}*A* k_h—as product between initiation area (IA), the maximum value of the GIST soil thickness map (d_{max}) in the source area, and a correction factor k_h, applying the following equation:

$$\mathrm{Vol} = d_{max} * \mathrm{IA} * k_h \tag{12}$$

where:

- Vol = volume of displaced material in the initiation area (m^3)
- d_{max} = maximum depth of the initiation area (m)
- IA = area of the initiation area (m^2)
- k_h = correction factor experimentally determined equal to 0.672

Based on the field data, the relationship (12) assumes that the maximum depth of the initiation area corresponds to the maximum soil thickness. In fact, in the source areas of rapid flows activated on October 1, 2009 in the Messina area, after the landslides failure,

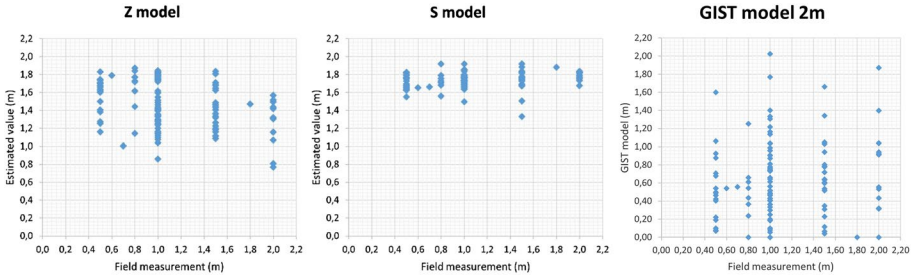

Fig. 10 Comparison between soil thickness field measurements (x axis) and Z (left), S (middle) and GIST (right) models' estimation (y axis)

the lithoid bedrock is often outcropping. The correction factor k_h was defined based on in-field measurements in eight initiation areas where the depths between the hypothetical original slope surface and the failure surface along 29 profiles were measured. The area of each section of the real profile was related to the corresponding "box-like" area, characterized by the maximum depth measured in the initiation area. The correction factor Kc constitutes the average value of the ratio between each real profile area and the "box-like" profile area (Fig. 11).

The four approaches were compared with the volume value estimated using Eq. (12); using this case, the maximum soil thickness values (d_{obs}) were observed during the in-field measurements in each source area (Table 1).

A comparison among the average of the differences between the values obtained with the assessed soil thickness and the in-field measures provides an estimate of the reliability of the four approaches (Table 2). The formula with the maximum value of soil thickness calculated in the initiation area with the GIST approach provides a volume value almost double that with the in-field measure, while the Volume Calculation Tool with the k_c correction factor provides a substantially inferior value. The results of the simple volume calculation tool, very similar to the volumes estimated through the average GIST values, provided volume values closer to the estimation with the field measures and consequently were preferred for the following elaboration.

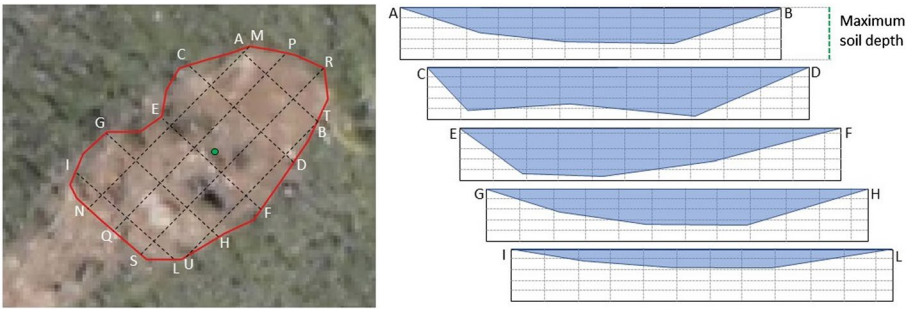

Fig. 11 In eight measured initiation areas, a maximum soil depth (green dot and line) was measured. Depth measurements in each initiation area permitted to draw several surfaces characterized by a horizontal hypothetical top line and by a measured bottom line. The k_h correction factor is the ratio between the sum of the all the surfaces and the sum of all the "box-like" area

Table 1 Measured and estimated soil thickness and calculated volumes of the source areas of the 50 elements of the training dataset (IA: initiation area; VCT: Volume Calculation Tool; d_{ave}: average depth estimated by the GIST model in the initiation area (m); d_{max}: maximum depth estimated by the GIST model in the initiation area (m); d_{obs}: maximum depth observed during the in-field measurements in the initiation area; k_h = correction factor experimentally determined)

LIP code	IA (m^2)	Soil thickness (m)			Estimated volume (m^3)				
		Field measure	Average GIST (d_{ave})	Maximum GIST (d_{max})	Method *I* (VCT)	Method II (VCT*K_h)	Method III (d_{ave}*IA)	Method IV (d_{max}*IA*kh)	Comparison model (d_{obs}*IA*K_h)
309	664	1.0	1.2	2.3	785	528	792	1023	446
401	310	0.6	0.6	1.1	180	121	185	239	125
405	304	1.0	0.3	1.2	109	73	106	250	204
464	244	2.0	0.2	0.6	48	33	53	106	328
465	444	2.0	0.8	2.2	354	238	365	663	597
475	33	0.5	0.4	0.7	10	7	12	15	11
477	778	1.0	1.3	3.2	937	630	973	1668	523
487	1156	1.0	1.0	2.5	1166	784	1208	1904	777
502	48	1.0	0.5	1.1	22	15	25	36	32
508	306	1.0	0.9	1.4	265	178	269	296	206
509	196	1.5	1.0	1.4	210	141	206	182	198
517	106	0.5	0.2	0.4	25	17	26	31	36
522	56	0.8	0.5	3.5	12	8	29	132	30
536	41	1.0	0.3	0.4	11	8	11	10	28
578	51	1.0	1.3	1.4	62	42	66	49	34
582	8	1.0	0.4	0.4	2	1	3	2	5
585	358	1.0	1.6	4.1	536	360	569	992	241
589	681	1.5	0.4	4.1	296	199	304	1890	686
611	794	1.0	0.7	2.1	561	377	556	1120	534
633	33	1.0	0.6	1.0	19	13	20	23	22
675	46	1.0	0.7	1.4	29	19	32	42	31
676	80	1.0	1.1	1.8	91	61	87	98	54

Table 1 (continued)

LIP code	IA (m^2)	Soil thickness (m)			Estimated volume (m^3)				
		Field measure	Average GIST (d_{ave})	Maximum GIST (d_{max})	Method *I* (VCT)	Method II (VCT*K_h)	Method III (d_{ave}*IA)	Method IV (d_{max}*IA*kh)	Comparison model (d_{obs}*IA*K_h)
711	1194	0.5	0.4	2.8	490	329	505	2243	401
762	83	1.0	0.5	0.8	38	26	39	44	56
765	169	0.8	0.8	1.6	115	77	128	182	91
767	25	0.5	0.6	0.7	12	8	14	11	8
768	92	1.0	0.9	1.2	82	55	83	75	62
773	172	1.0	1.1	1.2	182	122	185	143	116
776	207	1.0	0.5	0.9	110	74	113	121	139
777	35	1.0	0.7	0.8	21	14	24	20	24
802	9501	2.0	0.9	4.5	8551	5746	8681	28,725	12,769
803	283	2.0	0.6	0.9	160	107	164	176	380
830	42	1.0	0.6	0.8	18	12	24	22	28
831	276	1.5	2.0	4.5	467	314	554	830	278
832	61	1.5	1.7	2.7	110	74	105	112	61
833	130	1.5	1.1	1.7	152	102	142	151	131
844	811	2.0	0.7	2.1	570	383	571	1153	1090
897	43	0.5	0.6	1.0	33	22	27	30	14
901	596	1.0	0.4	1.1	244	164	245	434	401
940	6823	1.5	0.9	3.8	6078	4084	6216	17,578	6878
950	370	1.0	0.9	3.8	338	227	347	943	249
955	2163	2.0	0.9	4.5	1956	1314	2014	6502	2907
1045	6063	1.0	0.7	4.0	4214	2832	4273	16,500	4074
1152	1350	1.0	0.6	2.7	841	565	846	2438	907

Table 1 (continued)

LIP code	IA (m^2)	Soil thickness (m)			Estimated volume (m^3)				
		Field measure	Average GIST (d_{ave})	Maximum GIST (d_{max})	Method *I* (VCT)	Method II (VCT*K_h)	Method III (d_{ave}*IA)	Method IV (d_{max}*IA*kh)	Comparison model (d_{obs}*IA*K_h)
1213	390	1.5	0.9	2.0	332	223	347	517	393
1228	237	1,5	0,8	2	200	134	200	314	239
1248	343	1,5	1,1	1,5	361	242	372	357	346
1252	581	1	0,6	3,6	340	228	338	1408	390
1262	167	1,5	0,9	1,8	142	96	151	205	168
1322	83	1	1,1	1,9	88	59	92	107	56

Table 2 Volume estimation formula and value of the ratio between the estimated soil thickness and the in-field measurement

Formula	Estimated/field measured
Volume calculation tool GIST	1.05
Volume calculation tool GIST * k_h	0.7
Average GIST soil thickness * Area	1.10
Maximum GIST soil thickness * Area * k_h	1.82

From the linear elements layer of the observed runout, i.e., the paths of each landslide (LP), all the records were extracted singularly, thus obtaining fifty linear layers, each with a single path record, from which the relative topographic profile was produced. Along each profile, the SBP was manually identified, often with some difficulty: this element, in fact, is not always present or uniquely identifiable along the flow path. Nevertheless, the height (ΔH_s) and the planar (ΔX_s) distance between LIP and SBP for each flow has been identified (Fig. 12). Moreover, in a 4 m buffer (2 cell size radius) produced from each point of the SBP layer, the average slope values were calculated resulting in an overall value of 28°.

The three angular parameters α, β and θ included in the runout equations considered in the study, were evaluated using the slope map derived from the 2 m cell size DEM or through trigonometric calculations. The extension angle (α), as the angle between the horizontal and the line of conjunction between LIP and TP, was deduced as the arc-tangent of the ratio between the difference in height and the distance in plan between the two points (Fig. 13). The slope angle (θ) was obtained in the same way, using SBP instead of TP (Fig. 14). The transition angle (β, Fig. 15) was calculated as a function of the difference between the maximum and minimum angles identified in the 4 m buffer areas (2 cell size radius) produced from the SBP layer (Fig. 16).

Using the geometric and geographic features of LIP, SBP and TP of the fifty debris–mud flows of the training dataset, all the different geometric parameters correlated with the runout were defined.

The study was performed without considering the area and volume of the mobilized material outside the source area, i.e., in the track area (TA) along the landslide path (LP). Moreover, assuming by approximation that the type of mobilized material is uniform for all the landslides considered in the study, the Guo et al. (4) equation was simplified by attributing to the RT factor a constant value. Furthermore, this latter equation has been modified in order to make it easier to compare with the others:

$$L_{max} = e^{a} * e^{b*logV} * e^{c*\sin\beta} = e^{a} * V^{b} * e^{c*\sin\beta} \tag{13}$$

4 Results and discussion

The runout of the 50 observed phenomena of the training dataset, i.e., the length of the Landslide Path from each Initiation Area, was measured both in plan (L_{min}; 2D) and along the profile (L; 3D), providing non-negligible differences (average value: 22%; minimum: 6%; maximum: 44%; standard deviation: 9%; Fig. 17). This indicates the importance of

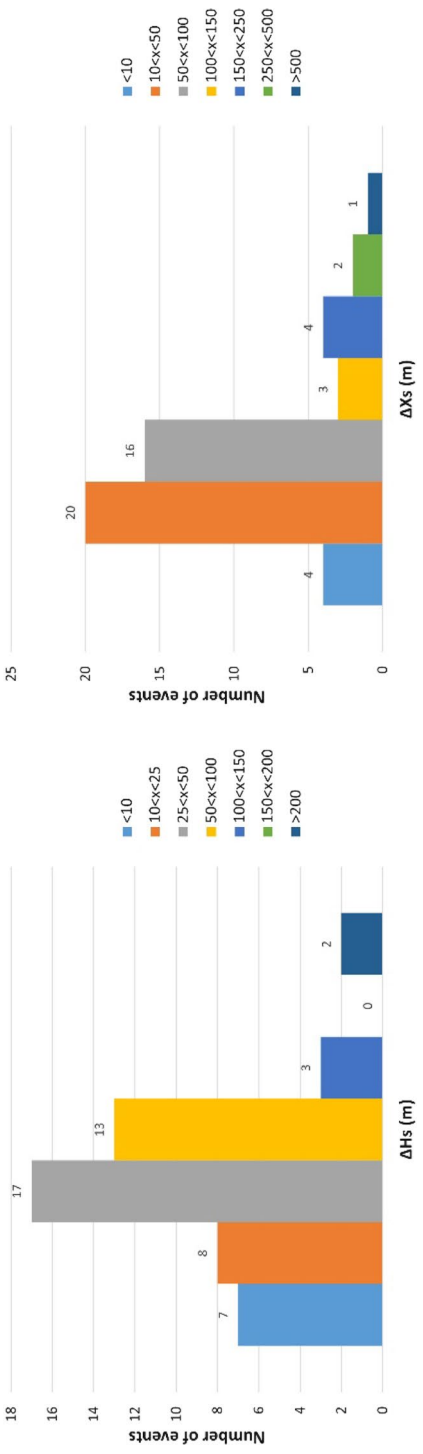

Fig. 12 Distribution of height (ΔH_s, left) and planar (ΔX_s, right) distance classes between LIP and SBP

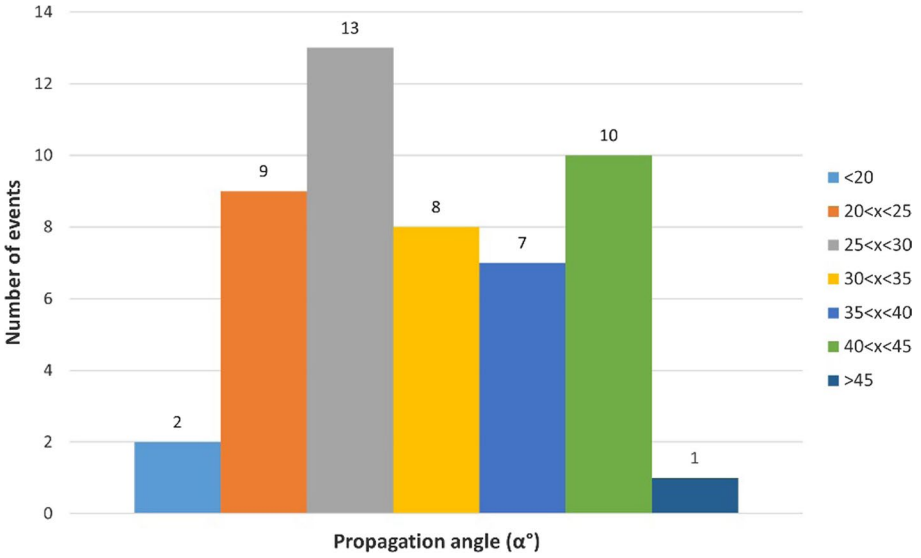

Fig. 13 Distribution of the propagation angle (α) classes in the 50 elements of the training dataset

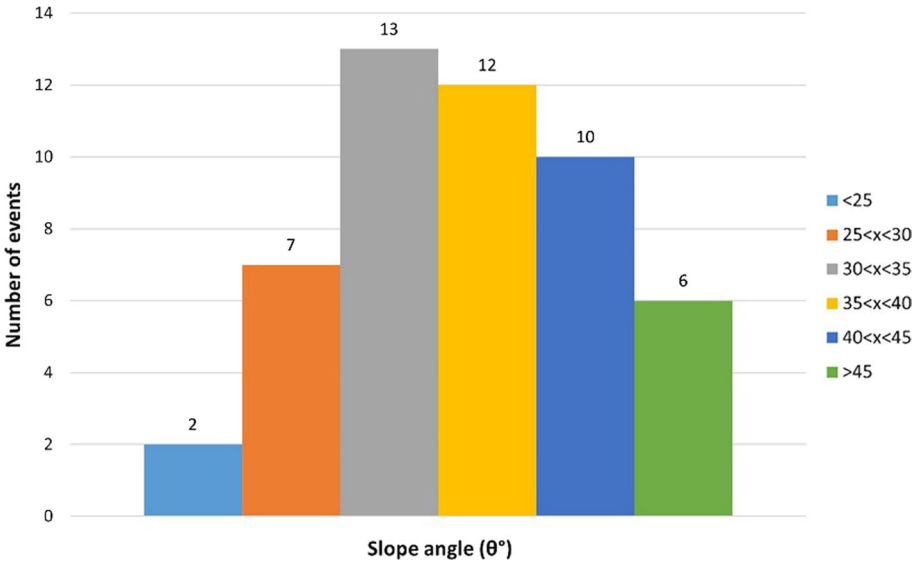

Fig. 14 Distribution of the slope angle (θ) classes in the 50 elements of the training dataset

clearly defining what type of runout distance it is calculating to avoid dangerous underestimates in forecasting analysis.

A correlation analysis among 2D and 3D runout and the landslide geometric characteristics was produced for each equation, using the volume calculated with the Volume

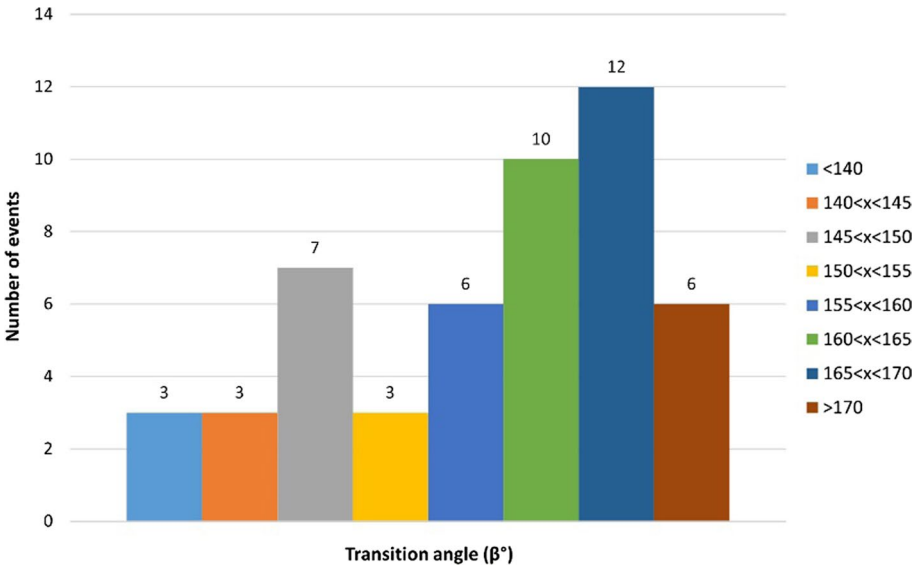

Fig. 15 Distribution of the transition angle (β) classes in the 50 elements of the training dataset

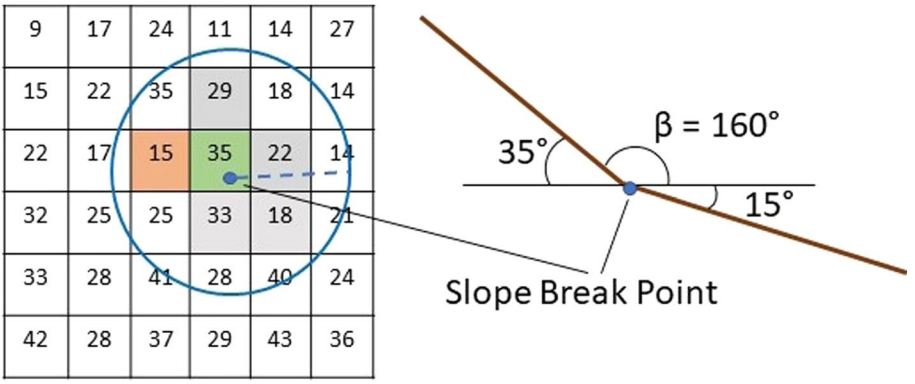

Fig. 16 The GIS query tool examines the cells entirely included in the buffer (blue lines) with the radius (blue dashed line) pointed in the Slope Break Point (blue dot) providing the minimum (orange cell) and the maximum (green cell) angles

Calculation Tool of QGIS (Fig. 18 and Table 3), both for confined and for unconfined landslides of the training dataset.

The five equations and related parameters taken from the training phase were then applied to the validation dataset. A comparison between observed and estimated runout values allows to evaluate the different performance of each equation (Figs. 19 and 20). Although the differences between the use of 2D and 3D length measures are very small in the training phase (Fig. 17), and given the greater simplicity of calculating the 2D distance compared to the 3D one, only the 2D length data were used for the validation analysis.

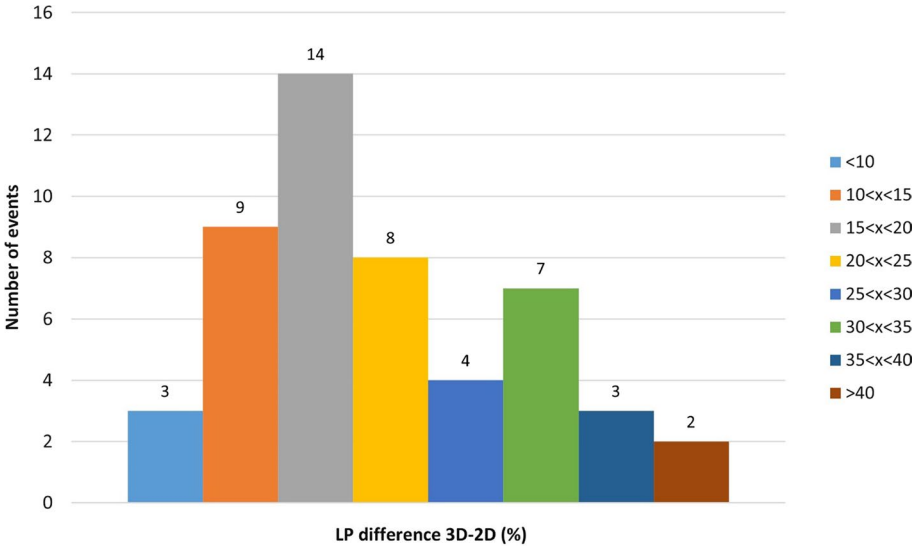

Fig. 17 Length % difference between 3 and 2D Landslide Path from each Initiation Area of the 50 elements of the training dataset

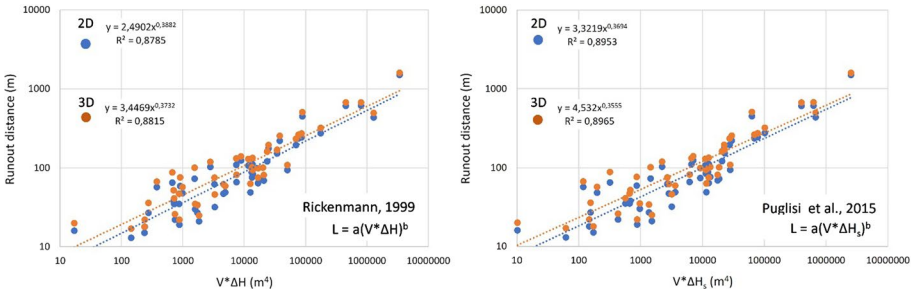

Fig. 18 Regression calculated using runout distance (*y* axis), both in 2D (blue dots) and 3D (orange dots), and the geometrical factors (*x* axis) considered in Rickenmann 1999 (left) and Puglisi et al. 2015 (right) equations, of the training dataset

Table 3 Power laws of each runout distance formula used in the study considering all the training landslide dataset (confined and unconfined), both in 2D and 3D

Complete dataset	2D equation	3D equation
Rickenmann (1999)	$L = 2.4902\ (V^{*}\Delta H)^{0.3882}$	$L = 3.4469(V^{*}\Delta H)^{0.3732}$
Legros (2002)	$L = 6.8959V^{0.4824}$	$L = 9.3935V^{0.4592}$
Guo et al. (2014)	$L = e^{0.7068} * V^{0.5904} * e^{1.7626 \mathrm{sen}\beta}$	$L = e^{1.0670} * V^{0.5665} * e^{1.6371 \mathrm{sen}\beta}$
Puglisi et al. (2015)	$L = 3.3219(V^{*}\Delta H_s)^{0.3694}$	$L = 4.532(V^{*}\Delta H_s)^{0.355}$
New equation	$L = 6.8424(V^{*}\Delta H_s/\Delta X_s)^{0.5171}$	$L = 9.1758(V^{*}\Delta H_s/\Delta X_s)^{0.4955}$

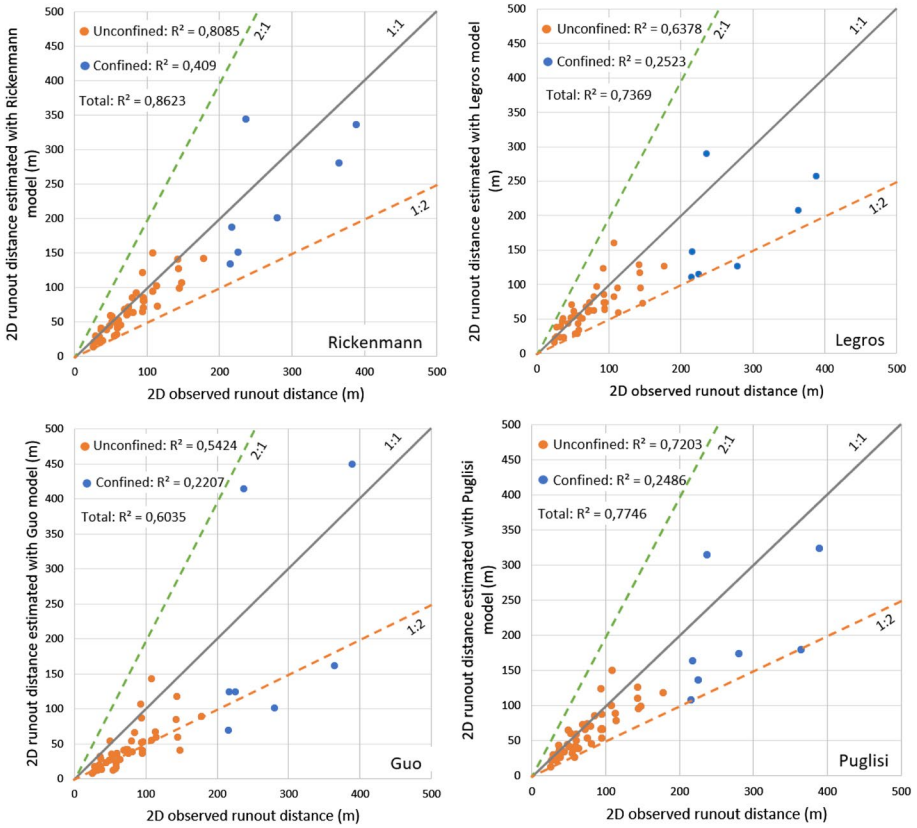

Fig. 19 Comparison between observed and estimated 2D runout distances calculated for the validation dataset with Rickenmann (1999), Legros (2002), Guo et al. (2014) and Puglisi et al. (2015) relationships: orange and blue dots are, respectively, related to unconfined and confined events

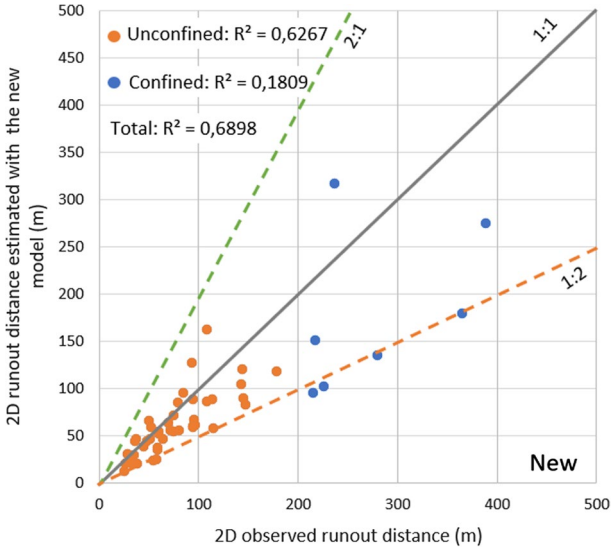

Fig. 20 Comparison between observed and estimated 2D runout distances with the new relationship

All the five relationships tend to underestimate the runout, particularly for the confined type, providing all positive values of the mean differences between observed and estimated propagation distance. The results of the entire validation dataset show high reliability in terms of R^2 of Eq. (5) (Puglisi et al. 2015), slightly lower than Eq. (2) (Rickenmann 1999). The other three equations ((3), (4) and (8)) provide lower R^2 values than (5). Although it introduces an additional variable (ΔX_s), the new Eq. (8) does not seem to provide a significant improvement in the forecasting capabilities of the geometric approach to runout estimation. The use of the tan(θ) instead of the $\Delta H_s/\Delta X_s$ ratio does not significantly modify the results. Even if Eq. (5) provides high performances, on the other hand the identification of the SBP was not yet obtained in automatic way and it is inevitably prone to subjective interpretation. The simplicity of the approach of Eq. (3), that relates the runout exclusively to the volume of the initiation area, makes it the easiest to use.

The separated analysis of the confined and unconfined landslide dataset leads to significant results. The R^2 values of the "unconfined" data (43 events) are similar to those of the "total" dataset, while for the "confined" data (7 events) R^2 values are substantially lower. The scattered effect complies with the possible uncertainty of the base data since the identification of the TP is much easier for unconfined events than for confined ones. While the toe of the landslide deposits is always well identifiable for unconfined debris flows, the TP of confined phenomena could be placed between the entrance into the main hydrographic network and the point where the deposited material is recognized: in the first case, the observed runout would probably be underestimated while in the second the effect of the hydraulic dynamics in the watercourse could be erroneously summed.

How to use data relating to multiple confined phenomena in which displaced material, coming from different and separated initiation areas, converge toward a single path, remains another open issue. In fact, it is difficult to attribute univocally part of the displaced material to different initiation area, when different surges share the same path. Similarly, summing the volumes of all the initiation areas in a single event could overestimate the volume of each event, attributing the sum to a single LIP. Five of the twelve confined landslides of the training dataset were highly multi-lobed and created serious interpretative problems, both for the estimate of the volume and for the location of the toe point. In these few cases (10% of the total), whose toe point corresponds to huge debris accumulations in the main valley floors, if not directly on the coast, the volume of a multiplicity of distinct scarps with strictly converging paths was attributed to a single LIP. Although it could overestimate the volume of some considered events, this approach was adopted in a precautionary way, permitting to contemplate in the comparison analysis even in extreme cases.

5 Conclusions

The empirical geometric approach finds its most appropriate application in the maps production for territorial planning and (pre)early warning systems, rather than for the design of protection works. Unfortunately, shallow landslide hazard maps containing runout estimation are currently not particularly widespread. In this study, the use of some empirical geometric runout equations allowed testing their specific reliability in the specific context of the Messina area.

Various approximation elements were introduced in the application of the five relationships. Firstly, the area and volume of the mobilized mass outside the initiation area, i.e.,

along the path, were not considered. Furthermore, the study made use of Eq. (3) assuming that the type of mobilized material was homogeneous for all the shallow landslide dataset.

The results show that 2D and 3D estimations are very similar in terms of reliability. Considering that all the five used equations tend to underestimate the runout distances, further improvements in the evaluation of the soil thickness with the GIST method may lead to providing more conservative predictions. Alternatively, the use of different volume calculation options may allow modulating distinguished expected scenarios.

The two functions (3) and (4), that introduced the use of the SBP, give acceptable results. If available, specific data on the lithological characteristics of the mobilized masses, expressed in the RT factor, may certainly contribute to achieving even better results. Furthermore, the implementation of an automatic and consistent GIS tool for placing the SBP along the landslide path may better express the potential of these two functions. The Legros equation seems to join the reliability of the results with easiness of use, while the new equation needs further application to better verify its potential. Further efforts must be addressed to identify a unique method to extrapolate the parameters of multilobate-confined phenomena; in fact, how to attribute the specific volumes and the position of the TP to this kind of debris flow remains an open issue.

Moreover, to improve the effectiveness of the empirical geometric approach for estimating the runout of potential events, it is necessary to perform detailed field surveys (Lorente, 2003), possibly carried out immediately following the occurrence of the landslides, and laboratory tests on soil samples of the mobilized material (Hürlimann et al. 2015). New field measurement of geometric data, such as soil thickness and volume of the initiation areas, and in situ and laboratory geotechnical and physical test of the soil and of the mobilized material, would allow the development of more detailed general equations and more effective site-specific curves.

Notwithstanding a non-negligible scattering between expected and observed runout distances and some limitations in exporting the correlation curves derived from datasets obtained in a specific area (Rickenmann 1999), the use of the geometric approaches can significantly boost the implementation of susceptibility analyses. Joining the runout estimate with the evaluation of kinematic parameters, such as velocity and kinetic energy, may lead to more detailed definition of landslides hazard at river basin scale. Although the geometric approach tends to simplify the complex dynamics of debris and mud flows, any future progress in the use of runout equations may greatly contribute to risk mitigation, producing more significant maps for spatial planning and more efficient early warning systems.

Acknowledgements The authors wish to thank Filippo Catani (University of Padova, Italy) and Samuele Segoni (University of Firenze, Italy) for providing useful advice about the use and application of the GIST model. Special thanks are devoted to Lina Vitali (ENEA, Italy) for her valuable support on the statistical evaluation of the geometric parameters dataset.

Author contributions All authors contributed to the study conception and design. Field activities and dataset collection were mainly performed by LMF and CP. GIS analysis and data elaboration were mainly performed by LMF and LM. The first draft of the manuscript was written by LMF and GR, and all authors commented on previous versions of the manuscript. All authors read and approved the final manuscript.

Funding This work was carried out as part of the RAFAEL project co-financed by the Ministry of University and Research under the PON "Research and Innovation" 2014–2020 and FSC funds referred to the D.D. of 13 July 2017 n. 1735—Application ARS01_00305 "Smart Secure and Inclusive Communities" specialization area.

Declarations

Conflict of interest The authors have no relevant financial or non-financial interests to disclose.

References

Ardizzone F, Basile G, Cardinali M, Casagli N, Del Conte S, Del Ventisette C, Fiorucci F, Garfagnoli F, Gigli G, Guzzetti F, Iovine G, Mondini AC, Moretti S, Panebianco M, Raspini F, Reichenbach P, Rossi M, Tanteri L, Terranova O (2012) Landslide inventory map for the Briga and the Giampilieri catchments NE Sicily, Italy. J Maps 8(2):176–180. https://doi.org/10.1080/17445647.2012.694271

Aronica GT, Brigandi G, Morey N (2012) Flash floods and debris flow in the city area of Messina, northeast part of Sicily, Italy in October 2009: the case of the Giampilieri catchment. Nat Hazards Earth Syst Sci 12:1295–1309. https://doi.org/10.5194/nhess-12-1295-2012

Ballatore GP, Fierotti G (1967) Carta dei suoli della Sicilia. Soc. Geografica, Via delle Mantellate, 14 – Firenze

Basile G, Panebianco M (2011) Experimental alert model for hydrogeological risk: a case study in Sicily. In: Proceedings of the second world landslide forum: 3–7 October 2011, Rome

Berti M, Simoni A (2007) Prediction of debris flow inundation areas using empirical mobility relationships. Geomorphology 90:144–161

Carbone S, Messina A, Lentini F (2007) Note illustrative della carta geologica D'italia alla scala 1:50.000, Foglio 601 - MESSINA-REGGIO DI CALABRIA. S.EL.CA. s.r.l., Firenze

Casalbore D, Chiocci FL, Scarascia Mugnozza G, Tommasi P, Sposato A (2011) Flash-flood hyperpycnal flows generating shallow-water landslides at Fiumara mouths in Western Messina Strait (Italy). Mar Geophys Res 32:257–271. https://doi.org/10.1007/s11001-011-9128-y

Catani F, Segoni S, Falorni G (2010) An empirical geomorphology-based approach to the spatial prediction of soil thickness at catchment scale. Water Resources Res;46:W05508, https://doi.org/10.1029/2008WR007450

Chae BG, Kim WY, Seo YS, Song YS (2006) Development of a method to assess runout distance of debris. IAEG2006 Paper number 176

Ciampalini A, Raspini F, Bianchini S, Frodella W, Bardi F, Lagomarsino D, Di Traglia F, Moretti S, Proietti C, Pagliara P, Onori R, Corazza A, Duro A, Basile G, Casagli N (2015) The landslide geodatabase of the Messina Province: a tool in the civil protection emergency cycle. Rend. Online Soc. Geol. It. 35:70–73. https://doi.org/10.3301/ROL.2015.66

Corominas J (1996) The angle of reach as a mobility index for small and large landslides. Geology. Canadian Geotechnical Journal

Corominas J, Copons R, Vilaplana JM, Altimir J (2003) Amigó J (2003) Integrated landslide susceptibility analysis and hazard assessment in the Principality of Andorra. Nat Hazards 30:421–435

Corominas J, van Westen C, Frattini P, Cascini L, Malet JP, Fotopoulou S, Catani F, Van Den Eeckhaut M, Mavrouli O et al (2014) Recommendations for the quantitative analysis of landslide risk. Bull Eng Geol Env 73(2):209–263. https://doi.org/10.1007/s10064-013-0538-8

Crosta GB, Dal Negro P, Frattini P (2003) Soil slips and debris flows on terraced slopes. Nat Hazard 3:31–42

Del Ventisette C, Garfagnoli F, Ciampalini A, Battistini A, Gigli G, Moretti S, Casagli N (2012) An integrated approach to the study of catastrophic debris-flows: geological hazard and human influence. Nat. Hazards Earth Syst. Sci., 12, 2907–2922. www.nat-hazards-earth-syst-sci.net/12/2907/2012/. https://doi.org/10.5194/nhess-12-2907-2012

Di Napoli M, Di Martire D, Bausilio G, Calcaterra D, Confuorto P, Firpo M, Pepe G, Cevasco A (2021) Rainfall-induced shallow landslide detachment, transit and runout susceptibility mapping by integrating machine learning techniques and GIS-based approaches. Water 13:488. https://doi.org/10.3390/w13040488

Fiorillo F, Diodato N, Meo M (2018) Pagnozzi M (2018) Landslides and flash floods induced by the storm of 22nd November 2011 in northeastern Sicily. Environ Earth Sci 77:602. https://doi.org/10.1007/s12665-018-7788-5

García-Ruiz JM, Beguería S, Lorente A, Martí C (2002) Comparing debris flow relationships in the Alps and in the Pyrenees. Instituto Pirenaico de Ecología, Zaragoza, Spain

DeGuidi G, Scudero S (2013) Landslide susceptibility assessment in the Peloritani Mts. (Sicily, Italy) and clues for tectonic control of relief processes. Nat Hazards Earth Syst Sci 13:949–963. https://doi.org/10.5194/nhess-13-949-2013

Guinau M, Vilajosana I, Vilaplana JM (2007) GIS-based debris flow source and runout susceptibility assessment from DEM data: a case study in NW Nicaragua. Nat Hazards Earth Syst Sci 7:703–716

Guo D, Hamada M, He C, Wang Y, Zou Y (2014) 2014 An empirical model for landslide travel distance prediction in Wenchuan earthquake area. Landslides 11:281–291. https://doi.org/10.1007/s10346-013-0444-y

Guthrie R, Befus A (2021) Debris flow predictor: an agent-based runout program for shallow landslides. Nat Hazards Earth Syst Sci 21:1029–1049. https://doi.org/10.5194/nhess-21-1029-2021

Heim A (1932) Der Bergsturz und Menschenleben. Fretz und Wasmuth Verlag, Zürich

Huang Y, Cheng H (2017) A simplified analytical model for run-out prediction of flow slides in municipal solid waste landfills. Landslides 14:99–107. https://doi.org/10.1007/s10346-016-0688-4

Hungr O (1995) 1995 A model for the runout analysis of rapid flow slides, debris flows, and avalanches. Can Geotech J 32(4):610–623. https://doi.org/10.1139/t95-063

Hungr O, Leroueil S, Picarelli L (2014) The Varnes classification of landslide types, an update. Landslides 11:167–194. https://doi.org/10.1007/s10346-013-0436-y

Hürlimann M, Rickenmann D, Medina V, Bateman A (2008) Evaluation of approaches to calculate debris-flow parameters for hazard assessment. Eng Geol 102(2008):152–163

Hürlimann M, McArdell BW, Rickli C (2015) Field and laboratory analysis of the runout characteristics of hillslope debris flows in Switzerland. Geomorphology 232:20–32. https://doi.org/10.1016/j.geomorph.2014.11.030

Jakob M, Hungr O (2005) Debris-flow hazard and related phenomena. Springer, New York

Legros F (2002) The mobility of long-runout landslides. Eng Geol 63(2002):301–331

Lombardo L, Opitz T, Huser R (2018) Point process-based modeling of multiple debris flow landslides using INLA: an application to the 2009 Messin4a disaster. Stoch Env Res Risk Assess. https://doi.org/10.1007/s00477-018-1518-0

Lorente A, Beguer S, Bathurst JC, Garcia-Ruiz JM (2003) 2003 Debris flow characteristics and relationships in the Central Spanish Pyrenees. Nat Hazards Earth Syst Sci Copernic Publ Behalf Eur Geosci Union 3(6):683–691

Malerba, S Brustia, E, Campolo, D, Comerci, V, Falconi L, Gioè, C, Lucarini, M, Lumaca, S, Puglisi, C, Torre, A, 2015 Landslides inventory in the Messina Municipality area: integration of historical and field survey data Engineering Geology for Society and Territory - Volume 2, Landslide Processes. Springer International Publishing Switzerland, ISBN: 978–3–319–09057–3, pp 967–970

McDougall S (2017) 2014 Canadian Geotechnical Colloquium: Landslide runout analysis—current practice and challenges. Can Geotech J 54:605–620. https://doi.org/10.1139/cgj-2016-0104

Melo R, Zezere, JL (2017) Debris-flow failure and run-out susceptibility assessment in the Zêzere river basin (Serra da Estrela, Portugal). Revista Brasileira de Geomorfologia. https://doi.org/10.20502/rbg.v18i1.985

Napoli R, Crovato C, Falconi L, Gioè C (2015) soil water content and triggering of debris flows in the messina area (Italy): preliminary remarks engineering geology for society and territory – Volume 2, landslide processes. Springer International Publishing Switzerland, ISBN: 978–3–319–09057–3, pp 2113–2117

Nigro F, Pisciotta A, Perricone M, Favara R, Renda P, Cusimano G, Torre F (2011) Stima Della Pericolosità Potenziale Al Dissesto Idrogeologico Nella Provincia di Messina: Valutazione Preliminare. Giornale Dell'ordine Regionale Dei Geologi Di Sicilia 3:2011

Pastor M, Blanc T, Manzanal D, Drempetic V, Pastor MJ, Sanchez M, Crosta G, Imposimato S, Roddeman D, et al. (2012) Landslide runout: Review of analytical/empirical models for subaerial slides, submarine slides and snow avalanche. Numerical modelling. Software tools, material models, validation and benchmarking for selected case studies. SafeLand Deliverable 1.7, Revision 2

Porter M, Morgenstern N (2013) Landslide Risk Evaluation – Canadian Technical Guidelines and Best Practices related to Landslides: a national initiative for loss reduction Geological Survey of Canada, Open File 7312. https://doi.org/10.4095/292234

Puglisi C, Falconi L, Grauso S, Screpanti A, Verrubbi V, Zini A, Crovato C, Campolo D, Leoni G, Lumaca S, Malerba S, Brustia E, Comerci V, Lucarini M, Napoli R, Torre A, Pino P (2013) Valutazione della pericolosità da frana nel Territorio del Comune di Messina RT/2013/18/ENEA https://iris.enea.it/retrieve/handle/20.500.12079/6666/416/RT-2013-18-ENEA.pdf

Puglisi C, Falconi L, Gioè C, Leoni G (2015) Contribution to the runout evaluation of potential debris flows in Peloritani Mountains (Messina, Italy). engineering geology for society and territory - Volume 2, landslide processes. Springer International Publishing Switzerland, ISBN: 978–3–319–09057–3, pp. 509–513

Rickenmann D (1999) Empirical relationships for debris flows. Natural Hazards 19: 47–77.lio 2007, 1–9

Rickenmann D (2005) Runout prediction methods. In: Jakob M, Hungr O (eds) Debris-flow hazards and related phenomena. Springer, Berlin, pp 305–324

Saulnier GM, Beven K, Obled C (1997) Including spatially variable effective soil depths in TOPMODEL. J Hydrol 202:158–172. https://doi.org/10.1016/S0022-1694(97)00059-0

Scheidl C, Rickenmann D (2010) Empirical prediction of debris-flow mobility and deposition on fans. Earth surface processes and landforms. Earth Surf Process Landforms 35:157–173

Schilirò L, Esposito C, Scarascia Mugnozza G (2015a) Evaluation of shallow landslide-triggering scenarios through a physically based approach: an example of application in the southern Messina area (northeastern Sicily, Italy). Nat Hazards Earth Syst Sci 15:2091–2109. https://doi.org/10.5194/nhess-15-2091-2015

Schilirò L, Esposito C, Scarascia Mugnozza G (2015b) A deterministic approach for shallow landslide triggering scenarios in the southern Messina area (north-eastern Sicily, Italy). Rend. Online Soc Geol It 35(2015b):272–275. https://doi.org/10.3301/ROL.2015.118

Regione Siciliana (2004) Piano stralcio di Bacino per l'Assetto Idrogeologico (P.A.I.) della Regione Siciliana. Relazione generale. Assessorato Territorio e Ambiente – Dipartimento Territorio e Ambiente

Regione Siciliana (2009) Criteri di intervento per la messa in sicurezza del centro abitato di Giampilieri Superiore colpito dall'alluvione del 1° ottobre 2009. DESCRIZIONE DEI DISSESTI E DEGLI INTERVENTI IMMEDIATI NEL CENTRO ABITATO DI GIAMPILIERI SUPERIORE. RELAZIONE PRELIMINARE. UFFICIO DEL COMMISSARIO DELEGATO EX O.P.C.M. 10 ottobre 2009, n.3815. 23/11/2009

Zou Z, Xiong C, Huiming T, Criss RE, Su A (2017) Liu X (2017) Prediction of landslide runout based on influencing factor analysis. Environ Earth Sci 76:723. https://doi.org/10.1007/s12665-017-7075-x